

pubs.acs.org/acssensors Article

# Carbon-13 Radiofrequency Amplification by Stimulated Emission of Radiation of the Hyperpolarized Ketone and Hemiketal Forms of Allyl [1-13C]Pyruvate

Shiraz Nantogma, Henri de Maissin, Isaiah Adelabu, Abubakar Abdurraheem, Christopher Nelson, Nikita V. Chukanov, Oleg G. Salnikov, Igor V. Koptyug, Sören Lehmkuhl, Andreas B. Schmidt, Stephan Appelt, Thomas Theis, and Eduard Y. Chekmenev\*



Cite This: ACS Sens. 2024, 9, 770-780



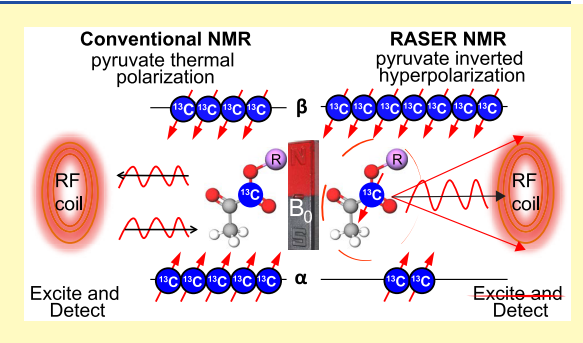
**ACCESS** 

III Metrics & More

Article Recommendations

Supporting Information

ABSTRACT: <sup>13</sup>C hyperpolarized pyruvate is an emerging MRI contrast agent for sensing molecular events in cancer and other diseases with aberrant metabolic pathways. This metabolic contrast agent can be produced via several hyperpolarization techniques. Despite remarkable success in research settings, widespread clinical adoption faces substantial roadblocks because the current sensing technology utilized to sense this contrast agent requires the excitation of <sup>13</sup>C nuclear spins that also need to be synchronized with MRI field gradient pulses. Here, we demonstrate sensing of hyperpolarized allyl [1-<sup>13</sup>C]pyruvate via the stimulated emission of radiation that mitigates the requirements currently blocking broader adoption. Specifically, <sup>13</sup>C Radiofrequency Amplification by Stimulated



Emission of Radiation (<sup>13</sup>C RASER) was obtained after pairwise addition of parahydrogen to a pyruvate precursor, detected in a commercial inductive detector with a quality factor (*Q*) of 32 for sample concentrations as low as 0.125 M with <sup>13</sup>C polarization of 4%. Moreover, parahydrogen-induced polarization allowed for the preparation of a mixture of ketone and hemiketal forms of hyperpolarized allyl [1-<sup>13</sup>C]pyruvate, which are separated by 10 ppm in <sup>13</sup>C NMR spectra. This is a good model system to study the simultaneous <sup>13</sup>C RASER signals of multiple <sup>13</sup>C species. This system models the metabolic production of hyperpolarized [1-<sup>13</sup>C]pyruvate, which has a similar chemical shift difference. Our results show that <sup>13</sup>C RASER signals can be obtained from both species simultaneously when the emission threshold is exceeded for both species. On the other hand, when the emission threshold is exceeded only for one of the hyperpolarized species, <sup>13</sup>C stimulated emission is confined to this species only, therefore enabling the background-free detection of individual hyperpolarized <sup>13</sup>C signals. The reported results pave the way to novel sensing approaches of <sup>13</sup>C hyperpolarized pyruvate, potentially unlocking hyperpolarized <sup>13</sup>C MRI on virtually any MRI system—an attractive vision for the future molecular imaging and diagnostics.

KEYWORDS: NMR, hyperpolarization, pyruvate, C-13, parahydrogen, laser, RASER

In NMR and MRI, there is a fundamental limitation posed on the attainable equilibrium nuclear spin polarization (P), i.e., the degree of nuclear spin alignment with an applied static magnetic field, under physiologically compatible conditions due to unfavorable Boltzmann statistics of nuclear spins that possess low magnetic moments. For example, proton, the most sensitive and abundant stable nuclear isotope, has an equilibrium P of only  $\approx 0.001\%$  at a clinically relevant 3 T field. Since the magnetic resonance (MR) signal is directly proportional to P, the major consequence of this limitation is the relatively low signal-to-noise ratio in NMR spectroscopy and its sister technology MRI. One way to overcome this low-P limitation is the use of NMR hyperpolarization techniques such as dissolution-dynamic nuclear polarization (d-DNP), spin-exchange optical pumping (SEOP),  $^{3,4}$  or parahydrogeninduced polarization (PHIP).  $^{5-7}$  All hyperpolarization techni-

ques have their own merits for production of hyperpolarized (HP) media, which can be used as exogenous contrast agents for molecular imaging.<sup>2,8–20</sup>

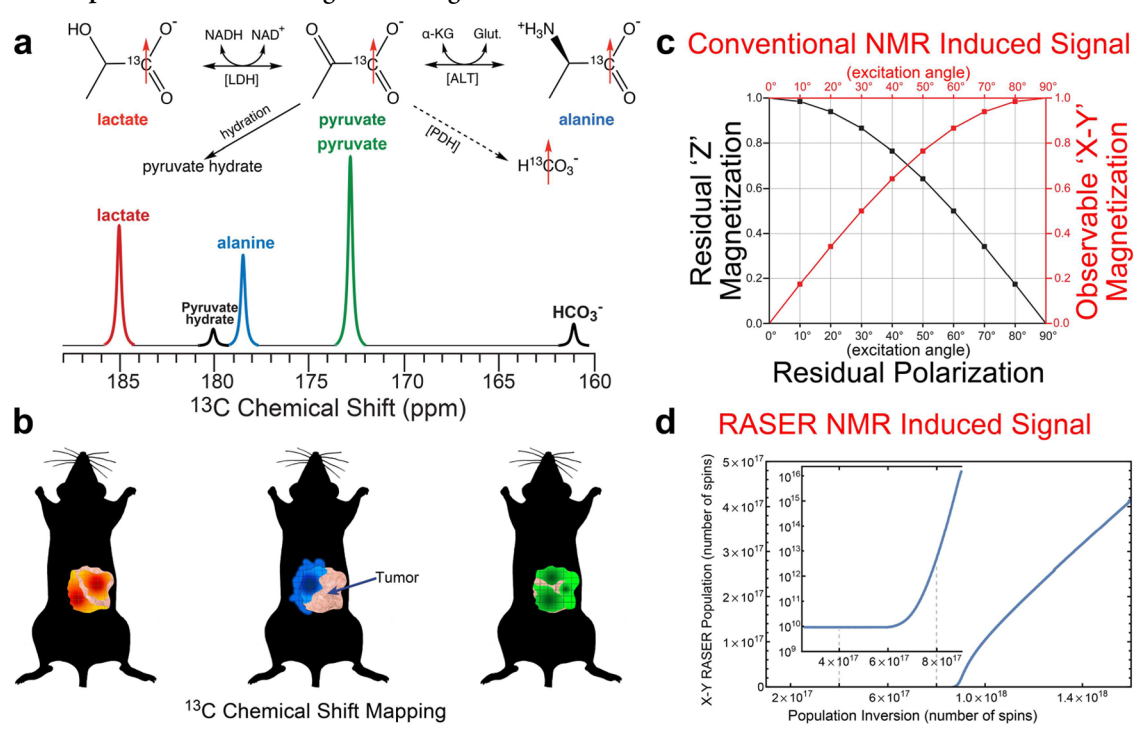
NMR hyperpolarization can create large inverted *P*, giving rise to unusual stimulated emissions in contrast with more conventional spontaneous emission employed in conventional NMR and MRI techniques. This stimulated emission phenomenon in MR is called Radiofrequency Amplification by Stimulated Emission of Radiation (RASER). RASER sensing

Received: October 1, 2023
Revised: December 12, 2023
Accepted: December 26, 2023
Published: January 10, 2024





Scheme 1. Concepts of HP Contrast Agent Sensing



"(a) In vivo administration of HP [1-13C]pyruvate leads to its in vivo uptake as well as its subsequent metabolism to [1-13C]alanine (by alanine transaminase [ALT]), [1-13C]lactate (by lactate dehydrogenase [LDH]), bicarbonate (by pyruvate dehydrogenase [PDH]) (followed by other downstream steps of oxidative phosphorylation schematically shown by a dashed line), and pyruvate hydrate (via hydration), which can be differentiated using <sup>13</sup>C NMR chemical shifts, and (b) detected using chemical shift mapping to simultaneously produce maps of multiple metabolites (three of which are shown schematically). Note the red (lactate), blue (alanine), and green (pyruvate) color coding in (a, b). (c) Trigonometric dependence of observed (sine) and remaining (cosine) magnetization as a function of RF pulse excitation (or "tipping") angle in spontaneous emission (i.e., conventional) NMR. (d) Simulations of <sup>13</sup>C RASER signal dependence (denoted as X–Y RASER population that produces NMR signal via inductive detection) on the population inversion. The inset shows the selected region of logarithmic scaling to emphasize the near-zero signal below the threshold level. Displays a, b, and c are reproduced with permission from ref 8. Copyright 2015 Wiley. Display d is reproduced with permission from ref 28. Copyright 2023 American Chemical Society.

offers a wide range of not yet fully realized advantages in sensing the MR signal over conventional NMR detection, including higher spectra precision because of narrower NMR lines, better fundamental resolution limits of MRI,<sup>23</sup> higher signal-to-noise ratio (SNR) because of the narrower lines, background-free detection,<sup>24</sup> and others.<sup>25</sup>

RASER has been demonstrated on a range on nuclear spins including protons, <sup>17</sup>O,<sup>26</sup> and more recently <sup>13</sup>C.<sup>27,28</sup> HP <sup>13</sup>C has a substantial biological relevance as it can be produced in a wide range of biologically relevant molecules, including most notably [1-<sup>13</sup>C]pyruvate.<sup>2</sup>

Several hyperpolarization techniques have succeeded in production and utilization of biocompatible <sup>13</sup>C HP contrast agents, including most prominently [1-<sup>13</sup>C]pyruvate, which has been hyperpolarized by d-DNP, <sup>2,18,29</sup> PHIP, <sup>30–36</sup> and signal amplification by reversible exchange (SABRE). <sup>9,19,20,37–40</sup> It should be noted that d-DNP is the leading hyperpolarization technique and the only one that has matured to clinical studies and clinical trials. Biocompatible HP [1-<sup>13</sup>C]pyruvate solution can be administered via injection, and, as illustrated in Scheme 1a, it is enzymatically converted mainly to HP [1-<sup>13</sup>C]alanine (via transamination <sup>41</sup>), [1-<sup>13</sup>C]lactate (via reduction <sup>41</sup>), <sup>13</sup>C-bicarbonate (via oxidative phosphorylation <sup>41</sup>), and [1-<sup>13</sup>C]-pyruvate hydrate (via hydration <sup>41</sup>) on the time scale of tens of seconds in vivo. <sup>19,20,41–45</sup> As illustrated in Scheme 1b, the chemical shifts of HP [1-<sup>13</sup>C]-pyruvate and its HP metabolic

products are different by as much as 12 ppm, and it becomes possible to distinguish each species via their chemical shift mapping.<sup>8</sup> For example, HP lactate mapping plays an important role in cancer imaging, 44,45 and bicarbonate mapping is also gaining interest for imaging oxidative phosphorylation as an emerging target in cancer therapy 46,47 and other applications.<sup>48</sup> One important advantage of RASER detection is that it does not require RF excitation, whereas conventional MR sensing requires the application of radio frequency (RF) pulses that excite nuclear spin magnetization (typically aligned along the main static magnetic field of the MR system (Z axis)). In conventional NMR or MRI, the RF pulse creates observable X-Y-magnetization, which is detected as an MR signal by the inductive detector. The RF excitation consumes the available Z-magnetization (Scheme 1c).8 Usually, multiple subsequent RF excitations are required for metabolic mapping (only one RF excitation is shown in Scheme 1c), and nonlinear pulsing schemes have been developed for more efficient metabolic mapping. 49 Since an HP state cannot be recovered in vivo, it decays exponentially to the typically nondetectable equilibrium level. The NMR signals that can be produced by the HP state must be captured on the time scale of  $T_1$  relaxation of the HP state, i.e., within 1-2 min for  $[1^{-13}C]$  pyruvate. A number of sensing approaches have been developed over the years, including traditional chemical shift imaging (CSI), which itself is now rarely used

with HP [1-13C]pyruvate. 50 More HP-magnetization efficient spectral-spatial excitation followed by a single-shot imaging readout (such as eco-planar imaging (EPI) or spiral imaging) has produced the highest-resolution images obtained with the HP [1-13C]pyruvate metabolic imaging technique by essentially undersampling in the spectral domain. 49-52 Moreover, the NMR signal created via XY-magnetization decays in accord with  $T_2^*$ , and this realization has led to the development of balanced steady-state free precession (SSFP) approaches to maximally "recycle" HP XY-magnetization for detection. 53,54 Furthermore, the trade-off about when to sample the HP Zmagnetization with respect to its  $T_1$  is a further optimization challenge—for example, the answer of "run at the shortest repetition time (TR)" of the MRI sequence is not necessarily optimal. The question of when to sample can be related to sampling theorems and the problems associated with kinetic rate constant estimation; e.g., HP bicarbonate produced from HP [1-13C]pyruvate injection has been imaged at a ~5 s temporal resolution to produce pH maps. 55 The main advantage of an increased TR is that one preserves comparatively more HP Z-magnetization for a period of time, where slower chemical kinetics may have occurred at the expense of  $T_1$  decay.

HP [1-13C]pyruvate contrast agent employs metabolic pathways similar to those of <sup>18</sup>F-fluorodeoxyglucose (<sup>18</sup>F-FDG). <sup>18</sup>F-FDG is widely employed in position emission tomography (PET) for molecular imaging of glucose uptake, which is elevated in many cancers 56,57 and other diseases 58 with elevated glucose metabolism. <sup>18</sup>F-FDG PET measures glucose uptake through GLUT transporters, and the radioactive label becomes stuck after phosphorylation by hexokinase; the assumption is that avid glucose uptake is synonymous with disease (although some tumors do not have elevated GLUT, and therefore, cannot be effectively imaged with <sup>18</sup>F-FDG). One practical limitation is the background physiological tissue uptake of <sup>18</sup>F-FDG, for example, by the brain and the prostate, thus limiting this tracer for applications in the brain and prostate cancer imaging, respectively. The molecular imaging scan with HP [1-13C]pyruvate has three critical translational advantages over <sup>18</sup>F-FDG-PET. It takes ~1 min compared to over 1 h (from injection to the end of the scan) and employs no ionizing radiation.<sup>59</sup> Moreover, HP [1-13C]pyruvate is taken up by monocarboxylate transporters, and the rate of label exchange with lactate depends on both the relative pool sizes of both moieties and the rate of consumption of HP [1-13C]pyruvate through PDH (Scheme 1); it is often said to reflect the rate of glucose oxidation, but strictly speaking this is not true. All in all, molecular imaging with the HP [1-13C]pyruvate contrast agent provides clinically useful, distinct information that is similar to that obtained by <sup>18</sup>F-FDG PET but directly probes relevant fluxes rather than just uptake. As a result, one can do meaningful HP [1-13C]pyruvate MRI for quantifying tumor metabolism in the human brain, where <sup>18</sup>F-FDG PET is widely regarded as nonspecific due to the high basal level of glucose uptake in the mammalian brain. These advantages make molecular MRI with HP [1-13C]pyruvate an important emerging molecular imaging technology. 45,60 Indeed, HP [1-13C] pyruvate is being evaluated for its efficacy in over 50 clinical trials according to clinicaltrials.gov.

However, because sensing of the HP [1-<sup>13</sup>C]pyruvate contrast agent and its metabolites requires the application of <sup>13</sup>C excitation pulses (Scheme 1), the metabolic MR exam with

injectable HP [1-13C]pyruvate contrast agent can only be performed on research MRI scanners that are equipped with specialized <sup>13</sup>C electronics needed for the excitation of <sup>13</sup>C nuclei. Conventional clinical MRI scanners are not equipped with such <sup>13</sup>C RF excitation/detection capability entirely, making the widespread biomedical translation of HP [1-13C]pyruvate challenging in a clinical workflow. While clinical MRI scanners can be upgraded to enable <sup>13</sup>C workflow, such upgrades are expensive (\$0.2-\$0.5M), have limited availability on vendors' scanner platforms, and are poorly integrated into the modern MRI clinical workflow: for example, unlike clinical proton workflow with dedicated transmit and receiver coils, the <sup>13</sup>C upgrade relies on transmit-receive coils, which have a number of disadvantages compared to separate transmit and receive coils approach employed in proton MRI. This translational challenge can be obviated using 13C RASER.<sup>28,61</sup> RASER<sup>22,62</sup> employs stimulated emission (predicted by Einstein<sup>63</sup>) created by population inversion. Unlike lasers employing population inversion of electronic states, RASER employs nuclear spin population inversion.<sup>22,62</sup> The "inverted" P of a sufficiently concentrated substrate gets coupled to the detector's resonating cavity leading to stimulated emission of radiation that can last for minutes. 21-26,61,64,65 A useful analogy is that the tuned RF circuit of a RASER acts like a mirror of a traditional LASER and partially reflects the virtual photons emitted by the nuclear spins. (We use the term "virtual" photons to refer to photons in the kHz to MHz regime, where the associated wavelengths exceed the physical dimensions of the coil. In the present case, the 15 MHz <sup>13</sup>C frequency is associated with a wavelength of about 20 m.) The current induced in the coil results in a backaction onto the spins leading to additional stimulated emission. The initial state before RASER activity is a strong population inversion, i.e., inverted (or negative) hyperpolarization. Random spin noise initially leads to the first emission events that lead to a back-action of the strongly coupled RF circuit eventually resulting in coherent emission of RF radiation. Even steady-state RASERs are possible, when providing continual pumping of hyperpolarization.<sup>66,67</sup> Remarkably, and in contrast to a typical LASER, the RASER dynamics are often dominated by the molecule and its nuclear spin system. 25,62,65 Therefore, molecule-specific information can be extracted easily and with unprecedented precision. 25,62,65

Another key translational advantage of a <sup>13</sup>C RASER over conventional HP MR detection is that it occurs without RF excitation (Scheme 1d). Once the inverted nuclear spin magnetization reaches the threshold given by eq 3, discussed in detail below (Scheme 1d), detectable X-Y magnetization is created as an observable NMR signal. One should note that there is virtually no signal below the threshold (corresponding to the "canonical" NMR regime), and once the threshold is exceeded, there is a linear dependence of stimulated emission in the X-Y plane as a function of inverted Z-magnetization. As discussed previously, this NMR spin system response is similar to the field-effect transistor (FET) current-voltage characteristics behavior, 28 where keeping the gate voltage below the switching threshold level maintains the transistor channel in the "off" position. On the other hand, exceeding this voltage switches the transistor channel "on" to the linear currentvoltage region.<sup>28</sup> Since the X-Y magnetization created by RASER results from the inverted HP spin state, it becomes possible to track chemical transformation of a bolus of HP <sup>13</sup>C compound without the use of RF excitation, if sufficient

inverted HP product has been created.<sup>28</sup> This is attractive for clinical MRI applications because dedicated high-power (typically 4 kW or more) transmitting RF coil and RF amplifiers are no longer required. Moreover, synchronization of transmit RF pulses and gradient pulses (needed for image encoding) is also no longer needed, potentially enabling encoding MRI pulse sequences for <sup>13</sup>C RASER using conventional proton pulse sequences already in place.<sup>28</sup> Our long-term goal is clinical translation of this promising technology to enable RASER sensing of HP [1-<sup>13</sup>C]pyruvate metabolism in vivo on virtually any MRI scanner by obviating the transmitting RF chain and the need for RF pulse synchronization with field gradient pulses. Our new envisioned approach requires only a high-Q low-power detector and preamplifier with ADC data recorder.<sup>28</sup>

Here, we demonstrate the feasibility of creating <sup>13</sup>C RASER using a bolus of HP allyl [1- $^{13}$ C]pyruvate $^{68}$  with inverted  $P_{13C}$ of 4% with a concentration as low as 0.125 M and a noncryogenic commercial detector with a quality factor of 32. While in this work, side arm hydrogenative PHIP<sup>68,69</sup> was employed to create the <sup>13</sup>C HP state on allyl [1-<sup>13</sup>C]pyruvate; other HP techniques, including SABRE-SHEATH 20,40 and d-DNP,<sup>2</sup> can also be readily employed to produce HP [1-13C]pyruvate for sensing of stimulated emission. Moreover, HP allyl [1-13C]pyruvate was produced in CD<sub>3</sub>OD, where it exists as two tautomers.<sup>68</sup> [1-<sup>13</sup>C] chemical shifts of these two tautomers differ by 10 ppm (i.e., similar to the chemical shift difference between [1-<sup>13</sup>C]pyruvate and [1-<sup>13</sup>C]lactate in vivo, the <sup>13</sup>C chemical shifts of which differ by 12 ppm, Scheme 1a), providing a well-controlled test system for two coexisting HP species with differing concentrations. We demonstrate that <sup>13</sup>C RASER signals can be created from both, one, or none of the species by controlling the 13C RASER threshold. These findings are important because they demonstrate the feasibility of multispecies RASER and more importantly RASER threshold control for background-free single-species RASER in the presence of other HP species. These results pave the way to future RASER sensing of [1-13C]pyruvate, its downstream metabolites, and other multinuclear HP contrast media.

# ■ MATERIALS AND METHODS

NMR Sample Preparation. Previously synthesized propargyl [1-13C]pyruvate was employed for all studies as an unsaturated precursor for pairwise addition of parahydrogen (p-H<sub>2</sub>). Samples were prepared by dissolving both propargyl [1-13C]pyruvate and Rh catalyst ((1,4-bis(diphenylphosphino)butane)(1,5-cyclooctadiene)rhodium(I) tetrafluoroborate, Strem P/N 45-0190, CAS 79255-71-3) in CD<sub>3</sub>OD to make a stock solution containing 1.0 M propargyl [1-13C]pyruvate and 10 mM Rh catalyst. This stock solution was then diluted to make sample solutions containing 62.5 125, 250, and 500 mM propargyl [1-13C]pyruvate and 0.63 1.3, 2.5, and 5.0 mM Rh catalyst, respectively. For <sup>13</sup>C polarization kinetics and temperature optimization studies, a solution containing 250 mM propargyl [1-13C]pyruvate and 4 mM Rh catalyst was freshly prepared by dissolving the required amounts of the substrate and catalyst in CD<sub>3</sub>OD. 0.6 mL of the prepared solution was pipetted into regularwall NMR tubes. Multiple samples were prepared from the same batch solution to systematically study the kinetics. All solutions were then purged with ultrahigh purity (>99.999%) argon for 1 min to remove any trapped air as described previously.<sup>61</sup>

<sup>13</sup>C Hyperpolarization of Allyl [1-1<sup>3</sup>C]Pyruvate via PHIP. The samples were hyperpolarized via pairwise p- $H_2$  addition to propargyl [1-1<sup>3</sup>C]pyruvate in the Earth's magnetic field that leads to production of proton-hyperpolarized allyl [1-1<sup>3</sup>C]pyruvate followed by polarization transfer from nascent p- $H_2$ -derived protons to the 1<sup>3</sup>C nucleus

via magnetic field cycling  $^{71}$  (Scheme 1a). A newly built integrated PHIP setup was employed for the hyperpolarization process, which is schematically shown in Scheme 1b. This polarizer employs compressed  $p\text{-}H_2$  gas with ~98% para-fraction, produced by a clinical-scale  $p\text{-}H_2$  generator. The sample loaded in an NMR tube was pressurized with  $p\text{-}H_2$  gas (100 psi overpressure provided by a safety release valve) and heated for a time period of 30–60 s at Earth's magnetic field. The sample was then bubbled with  $p\text{-}H_2$  gas for a time period  $T_{\text{hyd}}$  at a  $p\text{-}H_2$  flow rate of 150 standard cubic centimeters per minute (sccm) and quickly moved into a mu-metal shield, which was set to the residual static magnetic field of ~0.02  $\mu\text{T}$ , and then slowly pulled out in about 5 s to transfer polarization from protons to the  $^{13}\text{C}$  nucleus via magnetic field cycling as described previously. The sample of the property of the sample of the

Non-RASER <sup>13</sup>C NMR Data Acquisition. When the hyperpolarization process was completed, the HP sample in the NMR tube was manually transferred to a 1.4 T benchtop NMR spectrometer (SpinSolve Carbon, Magritek, New Zealand) for <sup>13</sup>C NMR signal detection. A <sup>13</sup>C spectrum was acquired with a 9° flip angle without proton decoupling and with a p-H $_2$  catheter present to prevent RASER activity (both of these factors decrease the effective  $T_2$ \*) (Figure 1a) (more detailed explanation is presented in the Results and Discussion section). An optimum temperature of 50 °C was found for the hyperpolarization process by varying the temperature of the water bath employed for sample heating during p-H $_2$  bubbling at the Earth's magnetic field. Similarly, polarization buildup studies were performed by varying the time of p-H $_2$  bubbling after heating the samples at a fixed temperature. An exemplary hydrogenation kinetic study is shown in Figure 1b.

**Computation of**  $P_{13C}$  **Values.** The non-RASER <sup>13</sup>C signal of the HP sample was compared to the <sup>13</sup>C signal of the reference compound (neat [1-<sup>13</sup>C]acetic acid at thermal equilibrium) to compute the  $P_{13C}$  value by taking into consideration the concentration of the sample  $C_{\rm HP}$ , the concentration of the reference sample ([1-<sup>13</sup>C]acetic acid),  $C_{\rm REF}$ , HP signal ( $S_{\rm HP}$ ), reference signal ( $S_{\rm REF}$ ), effective cross-section areas of the signal reference sample solution in the NMR tube and HP sample solution in the NMR tube,  $A_{\rm REF}$  and  $A_{\rm HP}$ , respectively, and <sup>13</sup>C thermal polarization at 1.4 T,  $P_{\rm therm}$  (eq 1).

$$P_{13C} = \frac{S_{\text{HP}}}{S_{\text{REF}}} \times \frac{C_{\text{REF}}}{C_{\text{HP}}} \times \frac{A_{\text{REF}}}{A_{\text{HP}}} \times P_{\text{therm}}$$
(1)

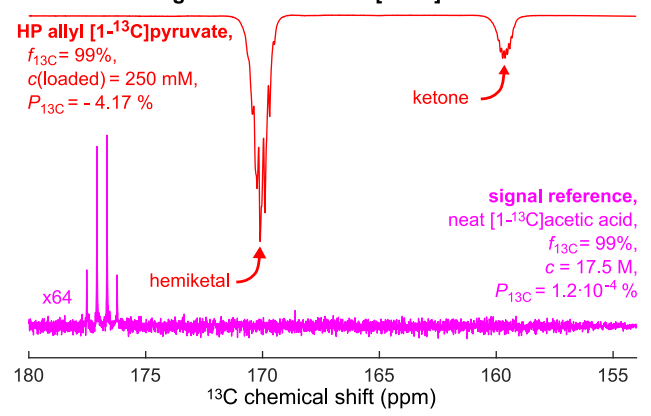
where  $P_{\rm therm}$  is  $1.2 \times 10^{-4}$ %,  $C_{\rm REF}$  is 17.5 M, and the ratio  $(A_{\rm REF}/A_{\rm HP})$  has been experimentally determined to be 1.03 for these experiments (the slight difference in the effective solutions' cross-section areas in 5 mm NMR tube (that affects the detected NMR signal) is due to placement of a Teflon catheter (for  $p\text{-H}_2$  gas delivery to the solution) in case of HP samples)—this value was measured by performing NMR signal integration on spectra obtained using thermally polarized samples with and without catheter placement.

<sup>13</sup>C RASER NMR Data Acquisition at 1.4 T. As described above, the HP allyl [ $1^{-13}$ C] pyruvate samples were quickly transferred to the spectrometer for  $^{13}$ C signal detection after completion of the hyperpolarization process.  $^{13}$ C detection using a low flip angle ( $9^{\circ}$ ) was done first without proton decoupling with the inserted p- $H_2$  bubbling catheter, both of which suppress  $^{13}$ C RASER activity. (A detailed experimental and theoretical study of  $^{13}$ C RASER control will be reported in the near future elsewhere; briefly, both catheter placement and NMR line splittings effectively decrease the  $T_2^*$  value of the NMR resonance resulting in the increase of  $P_{th}$  beyond what is obtained experimentally, eq 3.) This initial  $^{13}$ C detection, prior to RASER sensing, was needed for the quantification of  $P_{13C}$ . Then, the sample is pulled out of the spectrometer, the catheter is removed while simultaneously opening the spectrometer's receiver, and then, finally, the sample is inserted back into the spectrometer for  $^{13}$ C RASER acquisition with proton decoupling enabled.

 $^{13}$ C NMR Data Acquisition of  $^{13}$ C Polarization  $T_1$  Decay at 1.4 T Field. First, the  $^{13}$ C RASER signal was detected, as described above. Once the  $P_{13}$ C was below the RASER threshold, a separate pulse sequence protocol was loaded and employed to acquire a series

ACS Sensors pubs.acs.org/acssensors Article

# a 13C NMR spectroscopy of HP allyl [1-13C]pyruvate and 13C signal reference neat [1-13C]acetic acid



# hydrogenation kinetics c molar 13C polarization b -1 -2 0.8 P13C | · C (%·M) P13C (%) 0.6 0.4 -4 T<sub>hyd</sub>=9.5±1.3 s $T_{\rm rel} = 9.5 \pm 0.7 \text{ s}$ -5 0.2 $t_0$ =2.0±1.0 s =-10.8±0.3 % 0 -6 62.5 125 250 500 substrate concentration (mM) hydrogenation time (s) d hydrogenation kinetics model $P_{13C}(t_h) = \frac{P_{max}}{T_{hyd}/T_{rel} - 1} \cdot \left(\exp(-\frac{t_h - t_0}{T_{hyd}}) - \exp(-\frac{t_h - t_0}{T_{hyd}})\right)$

Figure 1. (a) (Top) Conventional (i.e., non-RASER)  $^{13}$ C NMR spectra of HP allyl [ $1^{-13}$ C]pyruvate produced from 250 mM sample of propargyl [ $1^{-13}$ C]pyruvate, showing the HP ketone and hemiketal forms; (bottom) corresponding signal reference spectrum from neat thermally polarized [ $1^{-13}$ C]acetic acid. (b) Recorded  $^{13}$ C polarization levels as a function of p-H $_2$  bubbling time after the sample tube was heated to 50 °C. (c) Molar polarization (provided as the product of loaded substrate concentration (assuming 100% chemical yield of the allyl product) and measured  $P_{13C}$  of allyl [ $1^{-13}$ C]pyruvate) obtained using a p-H $_2$  bubbling duration of 15 s and temperature of 50 °C at different starting concentrations of propargyl [ $1^{-13}$ C]pyruvate. (d) Equation for fitting hydrogenation kinetics used in (b) (derived elsewhere  $^{61,76}$ ).

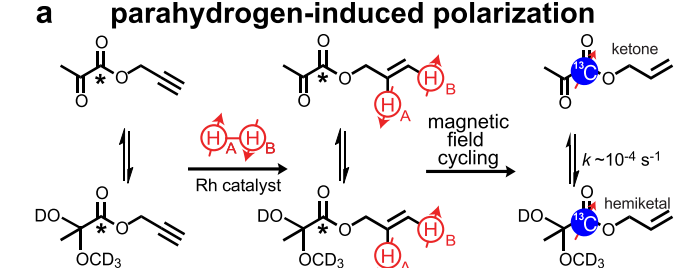
of non-RASER <sup>13</sup>C NMR spectra of HP allyl  $[1-^{13}C]$  pyruvate every 10 s with a pulse flip angle of 9°. The <sup>13</sup>C signals were integrated and corrected for polarization depletion due to n RF pulses using eq 2:

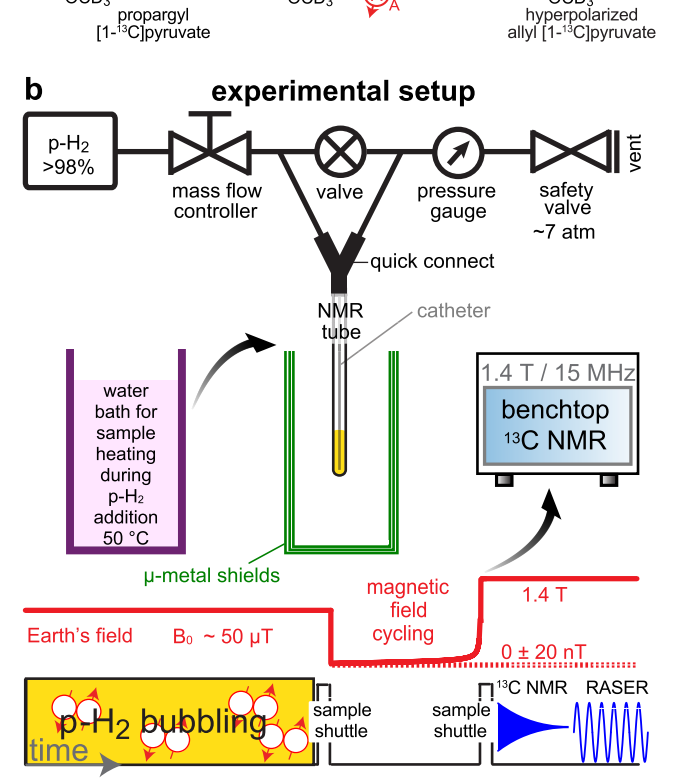
$$S(n) = S_{obs}(n)/(\cos(9^{\circ})^{n-1})$$
 (2)

where  $S_{obs}(n)$  is the observed <sup>13</sup>C signal intensity of the *n*th signal, S(n) is the corresponding corrected signal intensity, and  $n \geq 1$  is the <sup>13</sup>C signal acquisition number. The corrected in this fashion <sup>13</sup>C signal integral values were then fitted to a monoexponential decay function (Figure S2).

Measurement of Ketone and Hemiketal Exchange. Due to limited quantities of custom-made <sup>13</sup>C-enriched materials, a solution of structurally similar methyl pyruvate (Thermo Scientific, A1396614) in CD<sub>2</sub>OD was employed to estimate the exchange rate between ketone and hemiketal forms. A 0.4 mL aliquot of CD<sub>3</sub>OD was added to 0.2 mL of methyl pyruvate and quickly mixed immediately before sample insertion into the NMR spectrometer (1.4 T SpinSolve multi-X). The first <sup>1</sup>H spectrum was acquired approximately 0.5 min after mixing the liquids and approximately 10 s after sample insertion into the NMR spectrometer. A series of <sup>1</sup>H NMR spectra were acquired using a 9° flip angle for over 6 h (see SI for details). The addition of CD<sub>3</sub>OD leads to the formation of the hemiketal, which was not present in the pure methyl pyruvate liquid. Accordingly, the -CH<sub>3</sub> resonance of methyl pyruvate was used to detect the formation of the hemiketal and the disappearance of the ketone forms. Employing firstorder kinetics to model this process yielded an exchange rate constant magnitude of  $(9.4 \pm 0.4) \times 10^{-5}$  s<sup>-1</sup> (Figure S1). It should be noted that the effective rate constant of trifluoroacetaldehyde hemiacetalization in CD<sub>2</sub>OD was on the same order of magnitude ( $k \approx$  $3.5 \times 10^{-4} \text{ s}^{-1})^{77}$  despite the fact that the substrate structures were quite different. Therefore, the chemical exchange between the two allyl [1-13C]pyruvate tautomers shown in Scheme 2a was assumed to

Scheme 2. (a) Schematic of Pairwise Parahydrogen  $(p-H_2)$  Addition to Propargyl  $[1-^{13}C]$ Pyruvate Followed by Magnetic Field Cycling to Yield  $^{13}C$ -HP Allyl  $[1-^{13}C]$ Pyruvate in CD<sub>3</sub>OD and (b) Experimental Setup and Protocol Schematic





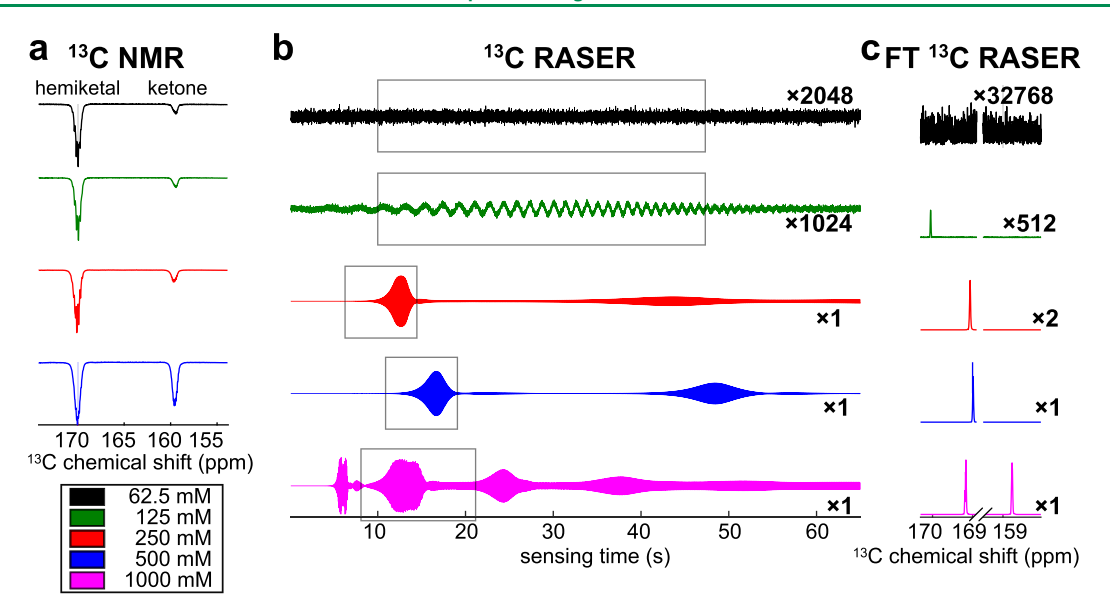


Figure 2. (a) Non-RASER  $^{13}$ C NMR spectra for evaluation of  $P_{13C}$  (not scaled), (b) corresponding  $^{13}$ C RASER FIDs acquired on the same samples, and (c) corresponding Fourier-transformed (FT) NMR spectra acquired for the samples with various starting concentrations of propargyl  $[1^{-13}$ C]pyruvate. Note the color coding of the sample concentrations: 62.5 mM (black), 125 mM (green), 250 mM (red), 500 mM (blue), and 1000 mM (magenta). The black boxes in display (b) denote the time regions over which the corresponding FT was performed in display (c). The illustrative example of the signal-to-noise ratio (SNR) for 500 mM sample yields SNR of 870 for hemiketal resonance (display a; acquired using a 9° flip angle), and the corresponding RASER resonance (shown in display c; acquired using no RF excitation) exhibits SNR of 220,000 (note the substantially broader lines of HP resonances in display a versus those in display c due to presence of a Teflon catheter, and the effect of the spin–spin couplings with protons—these compounding effects lead to lower SNR in the corresponding spectra shown in display a).

be similar to that between methyl pyruvate tautomers, i.e., on the time scale of  $10^4$  s, which is substantially greater than the time scale of  $^{13}$ C RASER emissions of  $\sim 10^2$  s.

# ■ RESULTS AND DISCUSSION

A fundamental requirement for stimulated emission of any kind is population inversion.  $^{63}$  In case of NMR-stimulated emission, the population inversion is established by the nuclear spins occupying Zeeman energy levels.  $^{62}$  As described previously, the stimulated emission of radiation from nuclear spins is created, when a sufficiently large population inversion (i.e., P < 0) exists in a resonant circuit.  $^{62}$  The RASER emission polarization threshold,  $P_{\rm th}$ , is given by  $^{61,62}$ 

$$P_{\rm th} = -4/(\mu_0 \hbar \eta \cdot Q \cdot \gamma^2 \cdot n_{\rm S} \cdot T_2^*)$$
 (3)

where  $\mu_0$  is the vacuum permeability,  $\hbar$  is the reduced Planck's constant,  $\eta$  is the filling factor of the resonator, Q is the quality factor of the resonator,  $\gamma$  is the gyromagnetic ratio of a nuclear spin (e.g.,  $^{13}$ C here),  $n_S$  is the spin number density, and  $T_2^*$  is the transverse nuclear spin relaxation time.

Here, sufficiently high inverted  $^{13}$ C magnetization was created using PHIP, as shown in Scheme 2a. The pairwise addition of p-H $_2$  to propargyl  $[1^{-13}\text{C}]$ pyruvate leads to symmetry breaking of the nascent p-H $_2$  protons. The polarization is transferred to the  $^{13}$ C nucleus from the p-H $_2$ -derived protons via spin—spin coupling and magnetic field cycling.  $^{31}$ C,  $^{71}$ 1,74 Using the previously developed PHIP kinetics model (Figure 1d), $^{61}$ 76 the hyperpolarization process (temperature and duration of p-H $_2$  bubbling) was optimized to maximize the absolute value of  $P_{13}$ C ( $\sim$ 4%) (Figure 1b). Note that other hyperpolarization techniques (e.g., d-DNP $^2$  or SABRE $^{20,39,78}$ ) can be in principle employed to create a bolus of HP  $^{13}$ C with sufficiently high  $n_s$  to satisfy eq 3—however,

the produced HP state must be inverted to induce the RASER effect

In addition to a sufficiently large  $n_S$ , other experimental parameters such as Q and  $T_2$ \* must be favorable for the spin system to reach the RASER threshold. In practice, the <sup>13</sup>C nucleus is spin-spin coupled to neighboring protons resulting in the splitting of the resonances and effective decrease of  $T_2^*$ , i.e., making it more experimentally challenging to fulfill <sup>13</sup>C RASER requirements dictated by eq 3. In our experimental protocol, we applied a small angle excitation RF pulse to probe <sup>13</sup>C magnetization of each freshly prepared HP sample, indeed, revealing the presence of broad <sup>13</sup>C resonances (Figure 2a). No characteristic <sup>13</sup>C RASER emissions were observed in these experiments due to substantial NMR line broadening. Since <sup>13</sup>C RASER was suppressed in such an experiment, the integration of <sup>13</sup>C signal intensities allowed for quantification of  $P_{13C}$  and the product of  $P_{13C}$  and concentration (Figure 1c). Moreover, each 13C spectrum acquired in this fashion revealed the presence of two 13C resonances corresponding to the ketone and hemiketal forms of HP allyl [1-13C]pyruvate in line with previous PHIP studies.<sup>68</sup>

The initial  $P_{\rm 13C}$  assessment was performed for  $10-12~\rm s.$  During this time, polarization losses are relatively small: indeed, the application of a 9° excitation pulse only reduces polarization by a factor of 1.01, and the 12-s-long time delay reduces  $P_{\rm 13C}$  by less than a factor of 1.08 since  $^{13}$ C  $T_{\rm 1}$  of HP allyl [1- $^{13}$ C]pyruvate is  $148 \pm 1~\rm s$  (Figure S2). Since  $P_{\rm 13C}$  was largely retained after the completion of this first experiment, a second NMR acquisition was performed immediately on the same sample, where the  $^{13}$ C excitation pulse was disabled and proton decoupling was applied continuously throughout the 65.6-s-long acquisition (Figure 2b). Proton decoupling collapses the lines that are otherwise split by  $^{13}$ C- $^{1}$ H spin-spin couplings, resulting in an increase of the effective  $T_{2}^{*}$ ,

thus substantially reducing the  $P_{13C}$  RASER threshold requirement (eq 3)—indeed, characteristic RASER bursts were readily observed for all HP sample studies with concentrations ranging from 125 to 1000 mM (Figure 2b) (the corresponding spectrograph representations of the RASER FIDs are presented in Figure S3). The stimulated <sup>13</sup>C signal emission lasted for tens of seconds until the inverted <sup>13</sup>C polarization of the HP state has decayed to the value below the threshold (eq 3). No <sup>13</sup>C RASER emissions were observed for the 62.5 mM sample, suggesting that the RASER threshold lies between  $P_{13C}$ ·c (molar polarization) of 0.3 and 0.47 M·% (Figure 1c). The RASER signal amplitude of the HP species is highly nonlinear with respect to the emission threshold: virtually, no emission is observed below the threshold, while marginally exceeding the RASER threshold results in strong signal emission (Scheme 1d). This nonlinear sensor behavior is in sharp contrast with conventional NMR, where the observed signal is directly proportional to the concentration and polarization of detected molecules.

Closer inspection of <sup>13</sup>C RASER FT spectra shown in Figure 2c reveals that <sup>13</sup>C RASER emissions can be obtained from both tautomers <sup>13</sup>C resonances only if the RASER condition (eq 3) is fulfilled for each individual resonance, e.g., <sup>13</sup>C spectrum at 1000 mM concentration. Since hemiketal tautomer is the dominant form, it can establish RASER emission at overall lower total concentration of HP molecule, whereas the <sup>13</sup>C RASER threshold condition for less-abundant ketone form is fulfilled only at 1000 mM total concentration of HP molecule (assuming 100% chemical yield into the allyl product). This RASER behavior of the <sup>13</sup>C HP allyl [1-13C]pyruvate spin system is remarkable in comparison to conventional NMR as it allows selectively sensing strong <sup>13</sup>C signal emissions from only one 13C HP species even in the presence of another strongly <sup>13</sup>C hyperpolarized species. This observation and the feasibility of such selective <sup>13</sup>C RASER sensing is important in the context of future biomedical applications of <sup>13</sup>C RASER sensing. The <sup>13</sup>C resonances of two pyruvate tautomers are separated by ~10 ppm, i.e., similar to the chemical shift separation of [1-13C]pyruvate and downstream metabolites in vivo ([1-13C]alanine and [1-13C]lactate, Scheme 1a). A number of <sup>13</sup>C RASER control mechanisms can be envisioned to selectively sense HP metabolites in the future in addition to proton decoupling employed here. For example, frequency-selective <sup>1</sup>H decoupling, ultrahigh-Q resonators <sup>79,80</sup> that can be potentially tuned selectively to the HP resonances of interest and so on (active work in our collaborating laboratories).

The novelty of this study lies in the sensing of the HP pyruvate moiety with notable biomedical relevance compared to the previous RASER studies performed in the acetate moiety. <sup>24,28,61,64</sup> Moreover, the study presented here examines the feasibility of creating <sup>13</sup>C RASER emissions in the presence of other <sup>13</sup>C HP species unlike previous work that has focused on studying the proton RASER creation in the presence of thermally polarized background polarization of the solvent. <sup>24</sup> The other remarkable feature of this work is that the two RASER lines of keto and hemiketal forms do not collapse into one line; i.e., despite RASER-feedback action, the ability to distinguish the two forms is fully retained.

With respect to limitations of this study, these pilot  $^{13}$ C pyruvate RASER experiments were performed in CD<sub>3</sub>OD solutions at superphysiological concentrations. Moreover, the estimated  $T_2^*$  was  $\sim 1.4$  s,  $^{61}$  i.e., approximately an order of

magnitude greater than clinically relevant values. We anticipate that the use of high-Q detectors<sup>79</sup> (i.e., Q > 20,000 vs 32 employed here) will enable <sup>13</sup>C RASER detection under the physiologically relevant conditions of HP <sup>13</sup>C metabolites' levels to enable studies of chemical transformation of HP  $[1-^{13}C]$  pyruvate with inverted  $P_{13C}$ . Indeed, the envisioned next step is to employ HP allyl [1-13C]pyruvate or HP [1-<sup>13</sup>C]pyruvate to sense its conversion to HP [1-<sup>13</sup>C]lactate (e.g., enzymatically via LDH + NAD/NADH, or via a cell line) or HP <sup>13</sup>C-bicarbonate (e.g., via H<sub>2</sub>O<sub>2</sub> addition) through this technique. Moreover, one clear limitation of the study is the detection of stimulated emission signal bursts (Figure 2b, rather than monotonically changing signals), which make quantification of chemical kinetic rate constants with RASER challenging using the conventional MR detection hardware (employed in the presented studies). However, this is not a fundamental limitation of the technique, and a number of approaches can indeed be envisioned. One such approach is to employ the detector circuit with variable O to enable active real-time feedback of the RASER signal that would prevent burst behavior but would instead generate a steady-state RASER signal<sup>66,67</sup>—in this case, the kinetics information may be potentially obtained through Q modulation for RASER signal detection of each species. Addressing these limitations and developing novel sensing detectors are active focus of our partnering laboratories.

#### CONCLUSIONS

It was demonstrated that <sup>13</sup>C RASER signals can be produced from an HP [1-13C]pyruvate moiety at sample concentrations as low as 125 mM using a nonmodified commercial RF coil with a quality factor of 32. Since the produced HP allyl [1-13C]pyruvate was present in both ketone and hemiketal forms in solution, it was possible to demonstrate simultaneous <sup>13</sup>C stimulated emissions from two species when the <sup>13</sup>C RASER threshold was exceeded for both HP tautomer species. When the RASER threshold was exceeded only for one tautomer (hemiketal form), the stimulated emission was produced by that species alone, and zero 13C signal was observed for the other HP tautomer (ketone form), which remained below the RASER threshold. This nuclear spin resonance RASER behavior is vastly different from conventional excite-detect NMR spectroscopy. HP [1-13C]pyruvate is the leading <sup>13</sup>C HP contrast agent being evaluated in over 50 clinical trials according to clinicaltrials.gov. Combined with recent advances on the feasibility of RASER MRI<sup>23</sup> and the utility of <sup>13</sup>C RASER to track chemical transformation, <sup>28</sup> these results bode well for future translation—indeed, we are hopeful that RASER-active HP [1-13C]pyruvate may be potentially useful for molecular imaging sensing applications, thus obviating the need for 13C RF excitation hardware and software on clinical MRI scanners.

#### ASSOCIATED CONTENT

### Supporting Information

The Supporting Information is available free of charge at https://pubs.acs.org/doi/10.1021/acssensors.3c02075.

Additional experimental details, materials and methods, NMR spectra, and time-resolved NMR spectroscopy (PDF)

ACS Sensors pubs.acs.org/acssensors Article

#### AUTHOR INFORMATION

#### **Corresponding Author**

Eduard Y. Chekmenev — Department of Chemistry, Integrative Bio-Sciences (IBIO), Karmanos Cancer Institute (KCI), Wayne State University, Detroit, Michigan 48202, United States; Russian Academy of Sciences, 119991 Moscow, Russia; orcid.org/0000-0002-8745-8801; Email: chekmenevlab@gmail.com

#### **Authors**

Shiraz Nantogma – Department of Chemistry, Integrative Bio-Sciences (IBIO), Karmanos Cancer Institute (KCI), Wayne State University, Detroit, Michigan 48202, United States

Henri de Maissin — Division of Medical Physics, Department of Radiology, Medical Center, University of Freiburg, Freiburg 79106, Germany; Faculty of Medicine, University of Freiburg, Freiburg 79106, Germany; German Cancer Consortium (DKTK), Partner Site Freiburg and German Cancer Research Center (DKFZ), Heidelberg 69120, Germany

Isaiah Adelabu — Department of Chemistry, Integrative Bio-Sciences (IBIO), Karmanos Cancer Institute (KCI), Wayne State University, Detroit, Michigan 48202, United States; orcid.org/0000-0002-9475-0851

Abubakar Abdurraheem — Department of Chemistry, Integrative Bio-Sciences (IBIO), Karmanos Cancer Institute (KCI), Wayne State University, Detroit, Michigan 48202, United States

Christopher Nelson – Department of Chemistry, North Carolina State University, Raleigh, North Carolina 27695, United States

Nikita V. Chukanov – International Tomography Center SB RAS, 630090 Novosibirsk, Russia

Oleg G. Salnikov – International Tomography Center SB RAS, 630090 Novosibirsk, Russia; orcid.org/0000-0003-2266-7335

Igor V. Koptyug – International Tomography Center SB RAS, 630090 Novosibirsk, Russia; Boreskov Institute of Catalysis SB RAS, 630090 Novosibirsk, Russia; orcid.org/0000-0003-3480-7649

Sören Lehmkuhl – Institute of Microstructure Technology, Karlsruhe Institute of Technology, Karlsruhe 76344, Germany; orcid.org/0000-0002-1321-7677

Andreas B. Schmidt — Department of Chemistry, Integrative Bio-Sciences (IBIO), Karmanos Cancer Institute (KCI), Wayne State University, Detroit, Michigan 48202, United States; Division of Medical Physics, Department of Radiology, Medical Center, University of Freiburg, Freiburg 79106, Germany; Faculty of Medicine, University of Freiburg, Freiburg 79106, Germany; German Cancer Consortium (DKTK), Partner Site Freiburg and German Cancer Research Center (DKFZ), Heidelberg 69120, Germany; orcid.org/0000-0001-8944-7463

Stephan Appelt – Institute of Technical and Macromolecular Chemistry, RWTH Aachen University, Aachen 52056, Germany; Central Institute for Engineering, Electronics and Analytics – Electronic Systems (ZEA-2), Jülich D-52425, Germany

Thomas Theis — Department of Physics and Joint UNC & NC State Department of Biomedical Engineering, North Carolina State University, Raleigh, North Carolina 27606, United States; orcid.org/0000-0001-6779-9978

Complete contact information is available at: https://pubs.acs.org/10.1021/acssensors.3c02075

#### **Notes**

The authors declare the following competing financial interest(s): Thomas Theis holds stock in Vizma Life Sciences LLC (VLS). EYC discloses a stake of ownership in XeUS Technologies, LTD. TT and EYC serve on the Scientific Advisory Board (SAB) of VLS. The terms of this arrangement have been reviewed and approved by NC State University in accordance with its policy on objectivity in research.

# ■ ACKNOWLEDGMENTS

This work was supported by National Institutes of Health grant R21EB025313 (T.T.), R01EB029829 (T.T.), and R21EB033872 (E.Y.C.) National Science Foundation grant: CHE-1904780 (E.Y.C.), WSU Thomas C. Rumble University Graduate Fellowship (S.N. and I.A.), the German Cancer Consortium (DKTK) (A.B.S.), WSU Competition for Postdoctoral Fellow award (A.B.S.), B.E.S.T. Fluidsysteme GmbH I Swagelok Stuttgart (A.B.S.), the Research Commission of the University Medical Center Freiburg (A.B.S.), the German Research Foundation (DFG) grants: #SCHM 3694/ 1-1, #SCHM 3694/2-1, and #SFB1479 (A.B.S.), the German Federal Ministry of Education and Research (BMBF) in the funding program "Quantum Technologies-from Basic Research to Market" under the project "QuE-MRT" contract number: 13N16448 (A.B.S.). O.G.S. thanks the Russian Science Foundation (Grant 21-73-10105) for support of preliminary PHIP studies with propargyl [1-13C]pyruvate. I.V.K. thanks RSF (grant #22-43-04426) for support of sample characterization with analytical techniques. The content is solely the responsibility of the authors and does not necessarily represent the official views of the National Institutes of Health. This material is based upon work supported by the U.S. Department of Energy, Office of Biological and Environmental Research (BER) under Award Number(s) DE-SC0023334. Disclaimer: This report was prepared as an account of work sponsored by an agency of the United States Government. Neither the United States Government nor any agency thereof, nor any of their employees, makes any warranty, express or implied, or assumes any legal liability or responsibility for the accuracy, completeness, or usefulness of any information, apparatus, product, or process disclosed, or represents that its use would not infringe privately owned rights. Reference herein to any specific commercial product, process, or service by trade name, trademark, manufacturer, or otherwise does not necessarily constitute or imply its endorsement, recommendation, or favoring by the United States Government or any agency thereof. The views and opinions of authors expressed herein do not necessarily state or reflect those of the United States Government or any agency.

## **■** REFERENCES

- (1) Hoult, D. I.; Richards, R. E. The signal-to-noise ratio of the nuclear magnetic resonance experiment. *J. Magn. Reson.* **1976**, 24 (1), 71–85.
- (2) Ardenkjaer-Larsen, J. H.; Fridlund, B.; Gram, A.; Hansson, G.; Hansson, L.; Lerche, M. H.; Servin, R.; Thaning, M.; Golman, K. Increase in signal-to-noise ratio of > 10,000 times in liquid-state NMR. *Proc. Natl. Acad. Sci. U. S. A.* **2003**, *100* (18), 10158–10163.
- (3) Walker, T. G. Fundamentals of Spin-Exchange Optical Pumping. J. Phys. Conf. Ser. 2011, 294, No. 012001.
- (4) Khan, A. S.; Harvey, R. L.; Birchall, J. R.; Irwin, R. K.; Nikolaou, P.; Schrank, G.; Emami, K.; Dummer, A.; Barlow, M. J.; Goodson, B. M.; Chekmenev, E. Y. Enabling Clinical Technologies for Hyper-

- polarized Xenon-129 MRI and Spectroscopy. Angew. Chem., Int. Ed. 2021, 60 (41), 22126-22147.
- (5) Bowers, C. R.; Weitekamp, D. P. Transformation of Symmetrization Order to Nuclear-Spin Magnetization by Chemical-Reaction and Nuclear-Magnetic-Resonance. *Phys. Rev. Lett.* **1986**, *57* (21), 2645–2648.
- (6) Eisenschmid, T. C.; Kirss, R. U.; Deutsch, P. P.; Hommeltoft, S. I.; Eisenberg, R.; Bargon, J.; Lawler, R. G.; Balch, A. L. Para Hydrogen Induced Polarization In Hydrogenation Reactions. *J. Am. Chem. Soc.* 1987, 109 (26), 8089–8091.
- (7) Kovtunov, K. V.; Pokochueva, E. V.; Salnikov, O. G.; Cousin, S.; Kurzbach, D.; Vuichoud, B.; Jannin, S.; Chekmenev, E. Y.; Goodson, B. M.; Barskiy, D. A.; Koptyug, I. V. Hyperpolarized NMR: d-DNP, PHIP, and SABRE. *Chem.—Asian J.* **2018**, *13* (15), 1857–1871.
- (8) Nikolaou, P.; Goodson, B. M.; Chekmenev, E. Y. NMR Hyperpolarization Techniques for Biomedicine. *Chem.—Eur. J.* **2015**, 21 (8), 3156–3166.
- (9) Schmidt, A. B.; de Maissin, H.; Adelabu, I.; Nantogma, S.; Ettedgui, J.; TomHon, P.; Goodson, B. M.; Theis, T.; Chekmenev, E. Y. Catalyst-Free Aqueous Hyperpolarized [1-<sup>13</sup>C]Pyruvate Obtained by Re-Dissolution Signal Amplification by Reversible Exchange. *ACS Sensors* **2022**, *7* (11), 3430–3439.
- (10) Hövener, J.-B.; Pravdivtsev, A. N.; Kidd, B.; Bowers, C. R.; Glöggler, S.; Kovtunov, K. V.; Plaumann, M.; Katz-Brull, R.; Buckenmaier, K.; Jerschow, A.; Reineri, F.; Theis, T.; Shchepin, R. V.; Wagner, S.; Bhattacharya, P.; Zacharias, N. M.; Chekmenev, E. Y. parahydrogen-based Hyperpolarization for Biomedicine. *Angew. Chem., Int. Ed.* **2018**, *57* (35), 11140–11162.
- (11) Brindle, K. M. Imaging Metabolism with Hyperpolarized <sup>13</sup>C-Labeled Cell Substrates. *J. Am. Chem. Soc.* **2015**, *137* (20), 6418–6427.
- (12) Schroder, L. Xenon for NMR biosensing Inert but alert. *Phys. Medica* **2013**, 29 (1), 3–16.
- (13) Witte, C.; Schroder, L. NMR of hyperpolarised probes. *NMR Biomed.* **2013**, 26 (7), 788–802.
- (14) Mugler, J. P.; Altes, T. A. Hyperpolarized <sup>129</sup>Xe MRI of the human lung. J. Magn. Reson. Imaging 2013, 37 (2), 313-331.
- (15) Walkup, L. L.; Woods, J. C. Translational applications of hyperpolarized <sup>3</sup>He and <sup>129</sup>Xe. NMR Biomed. **2014**, 27 (12), 1429–
- (16) Eills, J.; Budker, D.; Cavagnero, S.; Chekmenev, E. Y.; Elliott, S. J.; Jannin, S.; Lesage, A.; Matysik, J.; Meersmann, T.; Prisner, T.; Reimer, J. A.; Yang, H.; Koptyug, I. V. Spin Hyperpolarization in Modern Magnetic Resonance. *Chem. Rev.* **2023**, *123* (4), 1417–1551.
- (17) Ardenkjaer-Larsen, J.-H.; Boebinger, G. S.; Comment, A.; Duckett, S.; Edison, A. S.; Engelke, F.; Griesinger, C.; Griffin, R. G.; Hilty, C.; Maeda, H.; Parigi, G.; Prisner, T.; Ravera, E.; van Bentum, J.; Vega, S.; Webb, A.; Luchinat, C.; Schwalbe, H.; Frydman, L. Facing and Overcoming Sensitivity Challenges in Biomolecular NMR Spectroscopy. *Angew. Chem., Int. Ed.* 2015, 54 (32), 9162–9185.
- (18) Ardenkjaer-Larsen, J. H. On the present and future of dissolution-DNP. J. Magn. Reson. 2016, 264, 3-12.
- (19) MacCulloch, K.; Browning, A.; Guarin Bedoya, D. O.; McBride, S. J.; Abdulmojeed, M. B.; Dedesma, C.; Goodson, B. M.; Rosen, M. S.; Chekmenev, E. Y.; Yen, Y.-F.; TomHon, P.; Theis, T. Facile hyperpolarization chemistry for molecular imaging and metabolic tracking of [1–13C]pyruvate in vivo. *J. Magn. Reson. Open* **2023**, 16–17, No. 100129.
- (20) de Maissin, H.; Groß, P. R.; Mohiuddin, O.; Weigt, M.; Nagel, L.; Herzog, M.; Wang, Z.; Willing, R.; Reichardt, W.; Pichotka, M.; et al. In Vivo Metabolic Imaging of [1-<sup>13</sup>C]Pyruvate-d3 Hyperpolarized By Reversible Exchange With parahydrogen. *Angew. Chem., Int. Ed.* **2023**, *62*, No. e202306654.
- (21) Bear, D.; Chupp, T. E.; Cooper, K.; DeDeo, S.; Rosenberry, M.; Stoner, R. E.; Walsworth, R. L. Improved frequency stability of the dual-noble-gas maser. *Phys. Rev. A* **1998**, *57* (6), 5006–5008.
- (22) Suefke, M.; Lehmkuhl, S.; Liebisch, A.; Blumich, B.; Appelt, S. Para-hydrogen raser delivers sub-millihertz resolution in nuclear magnetic resonance. *Nat. Phys.* **2017**, *13* (6), 568–572.

- (23) Lehmkuhl, S.; Fleischer, S.; Lohmann, L.; Rosen, M. S.; Chekmenev, E. Y.; Adams, A.; Theis, T.; Appelt, S. RASER MRI Magnetic resonance images formed spontaneously exploiting cooperative nonlinear interaction. *Sci. Adv.* **2022**, *8* (28), No. eabp8483.
- (24) Joalland, B.; Theis, T.; Appelt, S.; Chekmenev, E. Y. Background-Free Proton NMR Spectroscopy with Radiofrequency Amplification by Stimulated Emission Radiation. *Angew. Chem., Int. Ed.* **2021**, *60* (50), 26298–26302.
- (25) Appelt, S.; Lehmkuhl, S.; Fleischer, S.; Joalland, B.; Ariyasingha, N. M.; Chekmenev, E. Y.; Theis, T. SABRE and PHIP pumped RASER and the Route to Chaos. *J. Magn. Reson.* **2021**, 322, No. 106815
- (26) Hope, M. A.; Björgvinsdóttir, S.; Grey, C. P.; Emsley, L. A Magic Angle Spinning Activated <sup>17</sup>O DNP Raser. *J. Phys. Chem. Lett.* **2021**, *12*, 345–349.
- (27) Nelson, C.; Schmidt, A. B.; Adelabu, I.; Nantogma, S.; Kiselev, V. G.; Abdurraheem, A.; de Maissin, H.; Lehmkuhl, S.; Appelt, S.; Theis, T.; Chekmenev, E. Y. parahydrogen-Induced Carbon-13 Radiofrequency Amplification by Stimulated Emission of Radiation. *Angew. Chem., Int. Ed.* **2023**, *62*, No. 202215678.
- (28) Schmidt, A. B.; Adelabu, I.; Nelson, C.; Nantogma, S.; Kiselev, V. G.; Zaitsev, M.; Abdurraheem, A.; de Maissin, H.; Rosen, M. S.; Lehmkuhl, S.; Appelt, S.; Theis, T.; Chekmenev, E. Y. <sup>13</sup>C Radiofrequency Amplification by Stimulated Emission of Radiation Threshold Sensing of Chemical Reactions. *J. Am. Chem. Soc.* **2023**, 145 (20), 11121–11129.
- (29) Ardenkjaer-Larsen, J. H.; Bowen, S.; Petersen, J. R.; Rybalko, O.; Vinding, M. S.; Ullisch, M.; Nielsen, N. C. Cryogen-free dissolution dynamic nuclear polarization polarizer operating at 3.35 T, 6.70 T, and 10.1 T. *Magn. Reson. Med.* **2019**, *81* (3), 2184–2194.
- (30) Cavallari, E.; Carrera, C.; Sorge, M.; Bonne, G.; Muchir, A.; Aime, S.; Reineri, F. The <sup>13</sup>C hyperpolarized pyruvate generated by parahydrogen detects the response of the heart to altered metabolism in real time. *Sci. Rep.* **2018**, *8* (1), 8366.
- (31) Reineri, F.; Boi, T.; Aime, S. parahydrogen Induced Polarization of <sup>13</sup>C carboxylate resonance in acetate and pyruvate. *Nat. Commun.* **2015**, *6*, 5858.
- (32) Hune, T.; Mamone, S.; Schroeder, H.; Jagtap, A. P.; Sternkopf, S.; Stevanato, G.; Korchak, S.; Fokken, C.; Müller, C. A.; Schmidt, A. B.; Becker, D.; Glöggler, S. Metabolic Tumor Imaging with Rapidly Signal-Enhanced 1-<sup>13</sup>C-Pyruvate-d3. *ChemPhysChem* **2023**, 24 (2), No. e202200615.
- (33) Nagel, L.; Gierse, M.; Gottwald, W.; Ahmadova, Z.; Grashei, M.; Wolff, P.; Josten, F.; Karaali, S.; Müller, C. A.; Lucas, S.; et al. Parahydrogen-Polarized [1-<sup>13</sup>C]Pyruvate for Reliable and Fast Preclinical Metabolic Magnetic Resonance Imaging. *Adv. Sci.* **2023**, *10*, No. 2303441.
- (34) Schmidt, A. B.; Bowers, C. R.; Buckenmaier, K.; Chekmenev, E. Y.; de Maissin, H.; Eills, J.; Ellermann, F.; Glöggler, S.; Gordon, J. W.; Knecht, S.; Koptyug, I. V.; Kuhn, J.; Pravdivtsev, A. N.; Reineri, F.; Theis, T.; Them, K.; Hövener, J.-B. Instrumentation for hydrogenative parahydrogen-Based Hyperpolarization Techniques. *Anal. Chem.* **2022**, *94* (1), 479–502.
- (35) Stewart, N. J.; Nakano, H.; Sugai, S.; Tomohiro, M.; Kase, Y.; Uchio, Y.; Yamaguchi, T.; Matsuo, Y.; Naganuma, T.; Takeda, N.; Nishimura, I.; Hirata, H.; Hashimoto, T.; Matsumoto, S. Hyperpolarized <sup>13</sup>C Magnetic Resonance Imaging of Fumarate Metabolism by parahydrogen-induced Polarization: A Proof-of-Concept in vivo Study. *ChemPhysChem* **2021**, *22* (10), 915–923.
- (36) Gierse, M.; Nagel, L.; Keim, M.; Lucas, S.; Speidel, T.; Lobmeyer, T.; Winter, G.; Josten, F.; Karaali, S.; Fellermann, M.; et al. parahydrogen-Polarized Fumarate for Preclinical in Vivo Metabolic Magnetic Resonance Imaging. *J. Am. Chem. Soc.* **2023**, *145* (10), 5960–5969.
- (37) Iali, W.; Roy, S. S.; Tickner, B. J.; Ahwal, F.; Kennerley, A. J.; Duckett, S. B. Hyperpolarising Pyruvate through Signal Amplification by Reversible Exchange (SABRE). *Angew. Chem., Int. Ed.* **2019**, *58* (30), 10271–10275.

- (38) Tickner, B. J.; Semenova, O.; Iali, W.; Rayner, P. J.; Whitwood, A. C.; Duckett, S. B. Optimisation of pyruvate hyperpolarisation using SABRE by tuning the active magnetisation transfer catalyst. *Catal. Sci. Technol.* **2020**, *10* (5), 1343–1355.
- (39) Adelabu, I.; TomHon, P.; Kabir, M. S. H.; Nantogma, S.; Abdulmojeed, M.; Mandzhieva, I.; Ettedgui, J.; Swenson, R. E.; Krishna, M. C.; Theis, T.; Goodson, B. M.; Chekmenev, E. Y. Order-Unity <sup>13</sup>C Nuclear Polarization of [1-<sup>13</sup>C]Pyruvate in Seconds and the Interplay of Water and SABRE Enhancement. *ChemPhysChem* **2022**, 23 (2), 131–136.
- (40) TomHon, P.; Abdulmojeed, M.; Adelabu, I.; Nantogma, S.; Kabir, M. S. H.; Lehmkuhl, S.; Chekmenev, E. Y.; Theis, T. Temperature Cycling Enables Efficient <sup>13</sup>C SABRE-SHEATH Hyperpolarization and Imaging of [1-<sup>13</sup>C]-Pyruvate. *J. Am. Chem. Soc.* **2022**, 144 (1), 282–287.
- (41) Golman, K.; in't Zandt, R.; Thaning, M. Real-time metabolic imaging. *Proc. Natl. Acad. Sci. U. S. A.* **2006**, *103* (30), 11270–11275. (42) Day, S. E.; Kettunen, M. I.; Gallagher, F. A.; Hu, D. E.; Lerche, M.; Wolber, J.; Golman, K.; Ardenkjaer-Larsen, J. H.; Brindle, K. M. Detecting tumor response to treatment using hyperpolarized C-13 magnetic resonance imaging and spectroscopy. *Nat. Med.* **2007**, *13* (11), 1382–1387.
- (43) Golman, K.; Petersson, J. S. Metabolic imaging and other applications of hyperpolarized C-13. *Acad. Radiol.* **2006**, *13* (8), 932–942.
- (44) Kurhanewicz, J.; Vigneron, D. B.; Brindle, K.; Chekmenev, E. Y.; Comment, A.; Cunningham, C. H.; DeBerardinis, R. J.; Green, G. G.; Leach, M. O.; Rajan, S. S.; Rizi, R. R.; Ross, B. D.; Warren, W. S.; Malloy, C. R. Analysis of Cancer Metabolism by Imaging Hyperpolarized Nuclei: Prospects for Translation to Clinical Research. *Neoplasia* 2011, 13 (2), 81–97.
- (45) Kurhanewicz, J.; Vigneron, D. B.; Ardenkjaer-Larsen, J. H.; Bankson, J. A.; Brindle, K.; Cunningham, C. H.; Gallagher, F. A.; Keshari, K. R.; Kjaer, A.; Laustsen, C.; et al. Hyperpolarized <sup>13</sup>C MRI: Path to Clinical Translation in Oncology. *Neoplasia* **2019**, *21* (1), 1–16.
- (46) Ashton, T. M.; McKenna, W. G.; Kunz-Schughart, L. A.; Higgins, G. S. Oxidative Phosphorylation as an Emerging Target in Cancer Therapy. *Clin. Cancer Res.* **2018**, *24* (11), 2482–2490.
- (47) Solaini, G.; Sgarbi, G.; Baracca, A. Oxidative phosphorylation in cancer cells. *Biochimica et Biophysica Acta (BBA)* -. *Bioenergetics* **2011**, 1807 (6), 534–542.
- (48) Merritt, M.; Harrison, C.; Storey, C.; Jeffrey, F.; Sherry, A.; Malloy, C. Hyperpolarized C-13 allows a direct measure of flux through a single enzyme-catalyzed step by NMR. *Proc. Natl. Acad. Sci. U. S. A.* **2007**, *104* (50), 19773–19777.
- (49) Miller, J. J.; Lau, A. Z.; Teh, I.; Schneider, J. E.; Kinchesh, P.; Smart, S.; Ball, V.; Sibson, N. R.; Tyler, D. J. Robust and high resolution hyperpolarized metabolic imaging of the rat heart at 7T with 3D spectral-spatial EPI. *Magn. Reson. Med.* **2016**, 75 (4), 1515–1524.
- (50) Yen, Y. F.; Kohler, S. J.; Chen, A. P.; Tropp, J.; Bok, R.; Wolber, J.; Albers, M. J.; Gram, K. A.; Zierhut, M. L.; Park, I.; Zhang, V.; Hu, S.; Nelson, S. J.; Vigneron, D. B.; Kurhanewicz, J.; Dirven, H.; Hurd, R. E. Imaging Considerations for In Vivo C-13 Metabolic Mapping Using Hyperpolarized C-13-Pyruvate. *Magn. Reson. Med.* **2009**, *62* (1), 1–10.
- (51) Cunningham, C. H.; Lau, J. Y. C.; Chen, A. P.; Geraghty, B. J.; Perks, W. J.; Roifman, I.; Wright, G. A.; Connelly, K. A. Hyperpolarized <sup>13</sup>C Metabolic MRI of the Human Heart. *Circ. Res.* **2016**, *119* (11), 1177–1182.
- (52) Gordon, J. W.; Autry, A. W.; Tang, S.; Graham, J. Y.; Bok, R. A.; Zhu, X.; Villanueva-Meyer, J. E.; Li, Y.; Ohilger, M. A.; Abraham, M. R.; Xu, D.; Vigneron, D. B.; Larson, P. E. Z. A variable resolution approach for improved acquisition of hyperpolarized 13C metabolic MRI. Magn. Reson. Med. 2020, 84 (6), 2943–2952.
- (53) Reed, G. D.; Morze, C. v.; Bok, R.; Koelsch, B. L.; Criekinge, M. V.; Smith, K. J.; Shang, H.; Larson, P. E. Z.; Kurhanewicz, J.; Vigneron, D. B. High Resolution <sup>13</sup>C MRI With Hyperpolarized Urea:

- In Vivo  $T_2$  Mapping and  $^{15}$ N Labeling Effects. *IEEE Trans. Med. Imaging* **2014**, 33 (2), 362–371.
- (54) Milshteyn, E.; von Morze, C.; Reed, G. D.; Shang, H.; Shin, P. J.; Larson, P. E. Z.; Vigneron, D. B. Using a local low rank plus sparse reconstruction to accelerate dynamic hyperpolarized <sup>13</sup>C imaging using the bSSFP sequence. *J. Magn. Reson.* **2018**, 290, 46–59.
- (55) Lau, A. Z.; Miller, J. J.; Tyler, D. J. Mapping of intracellular pH in the in vivo rodent heart using hyperpolarized  $[1-^{13}C]$  pyruvate. *Magn. Reson. Med.* **2017**, *77* (5), 1810–1817.
- (56) Fletcher, J. W.; Djulbegovic, B.; Soares, H. P.; Siegel, B. A.; Lowe, V. J.; Lyman, G. H.; Coleman, R. E.; Wahl, R.; Paschold, J. C.; Avril, N.; Einhorn, L. H.; Suh, W. W.; Samson, D.; Delbeke, D.; Gorman, M.; Shields, A. F. Recommendations on the Use of <sup>18</sup>F-FDG PET in Oncology. *J. Nucl. Med.* **2008**, 49 (3), 480–508.
- (57) Garcia, J. R.; Soler, M.; Blanch, M. A.; Ramirez, I.; Riera, E.; Lozano, P.; Perez, X.; Delgado, E.; Carrio, I.; Lomena, F. PET/CT with C-11-choline and F-18-FDG in patients with elevated PSA after radical treatment of a prostate cancer. *Rev. Esp. Med. Nucl.* **2009**, 28 (3), 95–100.
- (58) Bohnen, N. I.; Djang, D. S. W.; Herholz, K.; Anzai, Y.; Minoshima, S. Effectiveness and Safety of <sup>18</sup>F-FDG PET in the Evaluation of Dementia: A Review of the Recent Literature. *J. Nucl. Med.* **2012**, 53 (1), 59–71.
- (59) Nelson, S. J.; Kurhanewicz, J.; Vigneron, D. B.; Larson, P. E. Z.; Harzstark, A. L.; Ferrone, M.; van Criekinge, M.; Chang, J. W.; Bok, R.; Park, I.; et al. Metabolic Imaging of Patients with Prostate Cancer Using Hyperpolarized 1-C-13 Pyruvate. *Sci. Transl. Med.* **2013**, 5 (198), 198ra108.
- (60) Chung, B. T.; Chen, H.-Y.; Gordon, J.; Mammoli, D.; Sriram, R.; Autry, A. W.; Le Page, L. M.; Chaumeil, M. M.; Shin, P.; Slater, J.; Tan, C. T.; Suszczynski, C.; Chang, S.; Li, Y.; Bok, R. A.; Ronen, S. M.; Larson, P. E. Z.; Kurhanewicz, J.; Vigneron, D. B. First hyperpolarized [2-<sup>13</sup>C]pyruvate MR studies of human brain metabolism. *J. Magn. Reson.* **2019**, 309, No. 106617.
- (61) Nelson, C.; Schmidt, A. B.; Adelabu, I.; Nantogma, S.; Kiselev, V. G.; Abdurraheem, A.; de Maissin, H.; Lehmkuhl, S.; Appelt, S.; Theis, T.; Chekmenev, E. Y. parahydrogen-Induced Carbon-13 Radiofrequency Amplification by Stimulated Emission of Radiation. *Angew. Chem., Int. Ed.* **2023**, *62* (5), No. e202215678.
- (62) Appelt, S.; Kentner, A.; Lehmkuhl, S.; Blümich, B. From LASER physics to the para-hydrogen pumped RASER. *Prog. Nucl. Magn. Reson. Spectrosc.* **2019**, *114*–115, 1–32.
- (63) Einstein, A. Zur quantentheorie der strahlung. *Phys. J.* **1917**, *18*, 121–128.
- (64) Joalland, B.; Ariyasingha, N. M.; Lehmkuhl, S.; Theis, T.; Appelt, S.; Chekmenev, E. Y. parahydrogen-Induced Radio Amplification by Stimulated Emission of Radiation. *Angew. Chem., Int. Ed.* **2020**, *132* (22), *8732*–*8738*.
- (65) Lohmann, L.; Lehmkuhl, S.; Fleischer, S.; Rosen, M. S.; Chekmenev, E. Y.; Theis, T.; Adams, A.; Appelt, S. Exploring synchrony and chaos of parahydrogen-pumped two-compartment radio-frequency amplification by stimulated emission of radiation. *Phys. Rev. A* **2023**, *108* (2), No. 022806.
- (66) Yang, J.; Wang, P.; Korvink, J. G.; Brandner, J. J.; Lehmkuhl, S. The Steady-State ALTADENA RASER Generates Continuous NMR Signals. *ChemPhysChem* **2023**, 24 (14), No. e202300204.
- (67) TomHon, P. M.; Han, S.; Lehmkuhl, S.; Appelt, S.; Chekmenev, E. Y.; Abolhasani, M.; Theis, T. A Versatile Compact parahydrogen Membrane Reactor. *ChemPhysChem* **2021**, 22 (24), 2526–2534.
- (68) Salnikov, O. G.; Chukanov, N. V.; Shchepin, R. V.; Manzanera Esteve, I. V.; Kovtunov, K. V.; Koptyug, I. V.; Chekmenev, E. Y. parahydrogen-Induced Polarization of 1-<sup>13</sup>C-Acetates and 1-<sup>13</sup>C-Pyruvates Using Side-Arm Hydrogenation of Vinyl, allyl and propargyl Esters. *J. Phys. Chem. C* **2019**, *123* (20), *12827*–12840.
- (69) Švyatova, A.; Kozinenko, V. P.; Chukanov, N. V.; Burueva, D. B.; Chekmenev, E. Y.; Chen, Y.-W.; Hwang, D. W.; Kovtunov, K. V.; Koptyug, I. V. PHIP hyperpolarized [1-13C]pyruvate and [1-13C]-

- acetate esters via PH-INEPT polarization transfer monitored by <sup>13</sup>C NMR and MRI. Sci. Rep. **2021**, 11 (1), 5646.
- (70) Chukanov, N. V.; Salnikov, O. G.; Shchepin, R. V.; Kovtunov, K. V.; Koptyug, I. V.; Chekmenev, E. Y. Synthesis of Unsaturated Precursors for parahydrogen-Induced Polarization and Molecular Imaging of 1-<sup>13</sup>C-Acetates and 1-<sup>13</sup>C-Pyruvates via Side Arm Hydrogenation. *ACS Omega* **2018**, *3* (6), 6673–6682.
- (71) Johannesson, H.; Axelsson, O.; Karlsson, M. Transfer of parahydrogen spin order into polarization by diabatic field cycling. *C. R. Physique* **2004**, *5* (3), 315–324.
- (72) Nantogma, S.; Joalland, B.; Wilkens, K.; Chekmenev, E. Y. Clinical-Scale Production of Nearly Pure (>98.5%) parahydrogen and Quantification by benchtop NMR Spectroscopy. *Anal. Chem.* **2021**, 93 (7), 3594–3601.
- (73) Joalland, B.; Nantogma, S.; Chowdhury, M. R. H.; Nikolaou, P.; Chekmenev, E. Y. Magnetic Shielding of parahydrogen Hyperpolarization Experiments for the Masses. *Magn. Reson. Chem.* **2021**, 59 (12), 1180–1186.
- (74) Joalland, B.; Chekmenev, E. Y. Scanning Nuclear Spin Level Anticrossings by Constant-Adiabaticity Magnetic Field Sweeping of parahydrogen-Induced <sup>13</sup>C Polarization. *J. Phys. Chem. Lett.* **2022**, *13*, 1925–1930.
- (75) Nantogma, S.; Eriksson, S. L.; Adelabu, I.; Mandzhieva, I.; Browning, A.; TomHon, P.; Warren, W. S.; Theis, T.; Goodson, B. M.; Chekmenev, E. Y. Interplay of Near-Zero-Field Dephasing, Rephasing, and Relaxation Dynamics and [1-<sup>13</sup>C]Pyruvate Polarization Transfer Efficiency in Pulsed SABRE-SHEATH. *J. Phys. Chem. A* **2022**, *126* (48), 9114–9123.
- (76) Schmidt, A. B.; Berner, S.; Schimpf, W.; Müller, C.; Lickert, T.; Schwaderlapp, N.; Knecht, S.; Skinner, J. G.; Dost, A.; Rovedo, P.; Hennig, J.; von Elverfeldt, D.; Hövener, J. B. Liquid-state carbon-13 hyperpolarization generated in an MRI system for fast imaging. *Nat. Commun.* **2017**, *8*, 14535.
- (77) Salnikov, O. G.; Trofimov, I. A.; Pravdivtsev, A. N.; Them, K.; Hövener, J.-B.; Chekmenev, E. Y.; Koptyug, I. V. Through-Space Multinuclear Magnetic Resonance Signal Enhancement Induced by parahydrogen and Radiofrequency Amplification by Stimulated Emission of Radiation. *Anal. Chem.* **2022**, *94* (43), 15010–15017.
- (78) Barskiy, D. A.; Shchepin, R. V.; Tanner, C. P. N.; Colell, J. F. P.; Goodson, B. M.; Theis, T.; Warren, W. S.; Chekmenev, E. Y. The Absence of Quadrupolar Nuclei Facilitates Efficient <sup>13</sup>C Hyperpolarization via Reversible Exchange with parahydrogen. *ChemPhysChem* **2017**, *18*, 1493–1498.
- (79) Syms, R. R. A.; Floume, T.; Young, I. R.; Solymar, L.; Rea, M. Parametric Amplification of Magnetic Resonance Images. *IEEE Sens. J.* **2012**, *12* (6), 1836–1845.
- (80) Timilsina, R.; Fan, B.; Qian, C. Signal Sensitivity Enhancement of High-Spatial-Resolution MR Imaging with a Concatenated Cylindrical Parametric RF-Resonator. *IEEE Sens. J.* **2019**, *19* (9), 3431–3438.